

On the Flow Induced by Centrifugal Buoyancy in a Differentially-Heated Rotating Cylinder*

N. Brummell

Department of Astrophysical and Planetary Sciences, University of Colorado, Boulder, CO 80309, U.S.A.

J.E. Hart

Program in Atmospheric and Oceanic Sciences, University of Colorado, Boulder, CO 80309, U.S.A.

J.M. Lopez

Department of Mathematics, Arizona State University, Tempe, AZ 85287-1804, U.S.A.

Communicated by H.J.S. Fernando

Received 8 June 1999 and accepted 12 December 1999

Abstract. We consider the nature of thermally stratified flow in a closed cylinder rotating about the direction of gravity under conditions appropriate for terrestrial laboratory experiments. Motion is driven by centrifugal buoyancy, with outflow near the cold disk and inflow near the hot disk. Although similarity solutions for the infinite disk open-geometry problem exist and are easily found, even analytically in certain limits, there remain questions about the applicability of these spatially simplified models in a closed geometry with a vertical sidewall. This paper compares theoretical self-similar core solutions with computational simulations constructed to satisfy a wide range of sidewall thermal boundary conditions; insulating, conducting (with a linear temperature profile up the wall), hot (isothermal), or cold. The width of penetration of sidewall influence in toward the axis of rotation depends on the sidewall thermal boundary condition. However, as the cylinder radius is increased for a fixed height, a substantial region of the container about the axis is accurately described by the thermocline solutions of the theory. The non-self-similar region at large radius can include separation of the lower outflow boundary layer, a feature not evident in previous studies of this problem.

1. Introduction

Convectively unstable and stably stratified fluid dynamics experiments in rotating containers have a centrifugal buoyancy component perpendicular to the axis of rotation. In general this will induce a motion field that, in turn, modifies the distribution of temperature between the plates. The size and structure of this circulation is of interest to those performing rotating-stratified fluid experiments, as well as in engineering applications where rotationally induced buoyant motions may dominate over gravitational ones, for example, in rapidly rotating containers or in low to moderately rotating microgravity flows. The motion between differentially

* This research was sponsored by the National Science Foundation, Division of Atmospheric Sciences, under Grant ATM-97-14221 to the University of Colorado, and by support from NASA through its Microgravity Research Program, Grant NAG-3-1848.

heated rotating plates is also an important model problem for certain astrophysical and geophysical situations where isothermal boundaries are not geopotential surfaces.

Studies of stratified motions between infinite rotating disks were carried out by Duncan (1966) and by Hudson (1968). These authors use a slight variant of the standard similarity reduction for isothermal flow between infinite surfaces (e.g., Batchelor, 1951; Rogers and Lance, 1960) to reduce the full axisymmetric Navier-Stokes equations to a set of nonlinear ordinary differential equations (ODEs). Barcilon and Pedlosky (1967) and Homsy and Hudson (1969, 1971) addressed the effect of sidewalls on some of the similarity solutions. Barcilon and Pedlosky concluded that the core (i.e., away from the sidewall) behavior of the *linear problem* obtained from the similarity theory would not be significantly affected by a distant vertical sidewall. However, various informal arguments were presented to support their view that the so-called “thermocline,” or convectively dominated similarity solutions with strong vertical advection of temperature and narrow horizontal thermal boundary layers, could be seriously compromised. Indeed they state that the similarity solution may “not be the limiting solution (which we take to mean viable over most of the vessel) in a closed container, even with large radius.” Homsy and Hudson present asymptotic analysis in support of the view that for certain parameter settings, generally distinct from those used by Barcilon and Pedlosky, the self-similar core does exist. This analysis pivots on the assumption that the radial velocity in the outer radius region is small compared with the vertical velocity. This will not be the case, for example, if all or part of the horizontal boundary layer separates from the lower plate and enters the interior instead of running out to the lower corner and flowing directly up the sidewall. The present study suggests that the radial velocity can be significant near the outer wall in flows with typical laboratory parameter settings. Thus although the self-similar thermocline core can indeed appear in realistic situations, the flows in the outer region are different from those anticipated by these early works.

In this paper we recompute fully nonlinear solutions to the exact similarity reduction for the flow of a Boussinesq liquid between rapidly rotating isothermal, but differentially heated, horizontal boundaries. The theoretical analysis and the results presented from the computational simulations are restricted to the case of axisymmetric and steady motion. The transition, by instability, from a state that has the same symmetry as the container (i.e., circular) to full three-dimensional motion is an important issue for real systems. However, it is first necessary to understand the symmetric basic state, which in this instance is sufficiently complicated to warrant independent study by itself.

Some new aspects of the embedding of horizontal thermal and momentum boundary layers in the axisymmetric flow regime are displayed and discussed in terms of simple scaling arguments. The similarity solutions are then compared with the results of computational simulations of the axisymmetric circulation carried out in a finite geometry. Several values of the aspect ratio, the Froude number, the Rayleigh number, and various sidewall thermal boundary conditions are explored for the rapidly rotating (high Taylor number) regime. We focus on the stably stratified case where the top plate is hot and the bottom plate is cold. The case with a statically stable stratification allows for a larger imposed Rayleigh number, without setting off convective instabilities. This, in turn, means that strongly nonlinear centrifugal buoyancy effects may be observed directly, without interference from thermal convection on a small scale. A future paper will address the unstable (hot plate on the bottom) case, in which the interaction between a weak centrifugal circulation and convective instability at high wave number is the dominant feature.

The presentation is organized as follows. The self-similar model for the centrifugal buoyancy circulation is outlined in Section 2. The asymptotic weakly nonlinear solution for high Taylor number is summarized in Section 3. Numerical solutions of the reduced model are discussed in Section 4. Computational simulations of the full axisymmetric flow in a closed cylinder are described in Section 5, with conclusions following in Section 6.

2. Model Equations for Self-Similar Thermoclines

We study the axisymmetric motion between two parallel plates, rotating about their common axis at rate Ω , with the rotation vector being antiparallel to gravity. The disks are separated by a distance H and are differentially heated by raising the top temperature to $\Delta T/2$, and cooling the bottom to $-\Delta T/2$ (or vice versa for the unstably stratified case). The disks are infinitely conducting and they are bounded at radius

R by a vertical wall with various thermal properties that will be considered separately below. The relevant non-dimensional parameters are:

$$Ra = g\alpha\Delta TH^3/\kappa\nu, \quad (1a)$$

$$Ta = 4\Omega^2 H^4/\nu^2, \quad (1b)$$

$$Pr = \nu/\kappa, \quad (1c)$$

$$\Gamma = \alpha\Delta T/4, \quad (1d)$$

$$A = H/R, \quad (1e)$$

$$Fr = \Omega^2 R/g, \quad (1f)$$

being the Rayleigh, Taylor, and Prandtl numbers, density deficit, aspect ratio, and Froude number, respectively. Here α is the coefficient of expansion, ν is the kinematic viscosity, H is the layer depth, R is the cylinder radius, Ω is the rotation rate (antiparallel to the gravity g), κ is the thermal diffusivity, and ΔT is the applied temperature difference. In what follows, u is the radial, v is the azimuthal, and w is the vertical velocity, while p is the nondimensional fluctuating pressure normalized by the mean density ρ_0 . The dimensional scale factors are

$$H \text{ (for length), } \nu/H \text{ (for } u \text{ and } w), 2\Omega H \text{ (for } v), \text{ and } H^2/\nu \text{ (for time).} \quad (2)$$

The dimensional temperature field, taken to be statically stable if $\Delta T > 0$, is given by

$$T^* = \Delta T T_{\text{total}} = \Delta T [z^*/H + Pr T_c(r, z, t)], \quad (3)$$

where z^* is the dimensional height, which ranges between $-H/2$ and $H/2$, and T_c is the function representing the thermal deviation from the conductive state.

In the present calculation, the Boussinesq approximation has the same physical meaning as in the gravitational convection of a liquid. Density fluctuations only appear in terms reflecting the centrifugal acceleration associated with the basic rotation and with gravity. The density variation in the inertial terms is neglected, but does appear when multiplied by the centrifugal acceleration associated with the basic rotation, $\Omega^2 r$. This is presumed large compared with the centrifugal buoyancy arising from the relatively weak azimuthal motions measured relative to the state of rapid solid rotation. Alternatively, it is presumed the system has small Rossby number $V^*/2\Omega H \approx O(\Gamma) = O(\alpha\Delta T) \ll 1$, in which V^* is the azimuthal velocity measured relative to the basic rotation. V^* is small when the motion is driven by the relatively small density deficit obtainable in a liquid (see below).

Duncan (1966) and Hudson (1968) employ a reduction of the axisymmetric steady Navier–Stokes equations (written in rotating coordinates) that is similar to that historically employed in studies of flow between rotating disks (e.g., Batchelor, 1951; Rogers and Lance, 1960). It is useful to repeat this transformation explicitly. We write variables of the self-similar centrifugal circulation with subscript c . The deviation from the conduction temperature field, the relative velocities, and the pressure are written as

$$T = T_c(z), \quad u = rU_c(z), \quad v = rV_c(z), \quad w = W_c(z), \quad p = P_c(z) + r^2 Ta P_b/2, \quad (4)$$

where P_b is a constant to be determined, and z is the nondimensional height coordinate. Substitution of (4) into the Navier–Stokes equations in cylindrical coordinates results in a set of five nonlinear ordinary differential equations for the z -dependent parts of the solution. These are:

$$U_c^2 + W_c U_c' = (V_c^2 + V_c) Ta + U_c'' - \Gamma Ta(z + Pr T_c) - Ta P_b, \quad (5a)$$

$$U_c V_c + W_c V_c' = -(U_c V_c + U_c) + V_c'', \quad (5b)$$

$$Pr W_c T_c' = T_c'' - W_c, \quad (5c)$$

$$W_c' = -2U_c, \quad (5d)$$

$$P_c' = Ra T_c + W_c'' - W_c W_c'. \quad (5e)$$

Equation (5e), for the vertically varying pressure, is passive, so that P_c can be found after the vertical velocity and temperature fields are determined. As a result, the Rayleigh number does not enter as a determining parameter for the structure of the motion, although for fixed geometry and fluid properties it is directly

related to Γ . Equations (5a)–(5d) are subject to homogeneous rigid infinitely conducting boundary conditions on the three velocity components and the nonconductive part of the temperature field. These are

$$U_c = V_c = W_c = T_c = 0 \quad \text{at} \quad z = \pm \frac{1}{2}. \quad (6)$$

The fact that there are eight boundary conditions, while (5a)–(5d) is only seventh order, requires the addition of a barotropic radial pressure field, proportional to P_b , into the makeup of the solution. In physical terms (at large Taylor number), this pressure field, which appears as a forcing on the far right-hand side of (5a), is accompanied by a geostrophically balanced barotropic solid rotation flow in the interior. The Ekman layers associated with this interior swirl then drag fluid in from or out to infinity, thereby permitting maintenance of mass balance in the radial direction. Since the integral of the radial velocity across the entire layer then vanishes, (5d) guarantees that W vanishes at both walls if it vanishes at one.

3. The Weakly Nonlinear Circulation

An analytic approximation for the motion between infinite plates may be obtained by perturbation expansion in powers of the density deficit parameter Γ . The asymptotic form of this solution, valid at large Taylor number and through second order in Γ , is:

$$V_c = \Gamma z - \Gamma^2 z^2 + \Gamma^2 \text{Pr} \lambda (\frac{1}{4} - z^2)/2 + P_b, \quad (7a)$$

$$P_b = \Gamma^2 [\frac{17}{20} - 3/2\lambda + 1/\lambda^2 + \text{Pr}(1/2\lambda - \frac{1}{2})], \quad (7b)$$

$$U_c = \Gamma^2 [\lambda(1 - \text{Pr}) - 2], \quad (7c)$$

$$W_c = -\Gamma\lambda - 2\Gamma^2 [\lambda(1 - \text{Pr}) - 2]z, \quad (7d)$$

$$T_c = \Gamma\lambda(\frac{1}{8} - z^2/2) - \Gamma^2 [\lambda^2 \text{Pr}/6 + \lambda(\text{Pr} - 1)/3 + \frac{2}{3}](z^3 - z/4). \quad (7e)$$

Here, the inverse Ekman layer thickness $\lambda \equiv (\text{Ta}/4)^{1/4}$. Equations (7) describe the fields outside thin but linear Ekman boundary layers attached to the two plates. Due to approximations made in the analysis, these interior fields, including P_b , have errors of relative magnitude $O(\text{Ta}^{-1/4})$. The second-order solutions, proportional to Γ^2 , have the opposite symmetry, about $z = 0$, to that present in the linear (in Γ) solution. Thus the full solution is asymmetric. The second-order barotropic swirl (i.e., P_b) is nonzero.

Consider a realistic, or reasonably feasible, laboratory experiment with a low viscosity silicone oil (1 cs, say), a 10° thermal drop, and a 1 cm gap. The Prandtl number of such a fluid is about 8. In this situation, when the system rotates at a 10 s rotation period, the thermal perturbation, according to (7e), will be about 30% of the conductive values. Going to a 3 s period raises this to about 70%. With a 40° temperature drop, a 1 s rotation period, and a 2 cm gap, the thermal perturbation is about ten times the conductive maximum of 0.5. It is clear that under extreme conditions the centrifugal buoyancy circulation may become highly nonlinear, and even under moderate conditions it can significantly alter the conductive temperature distribution. A typical Froude number for a realistic laboratory experiment with a 20 cm radius ranges from about 0.1 to 0.7 as the period goes from 3 s to 1 s.

4. Numerical Results for Infinite Disks

Although Hudson (1968) obtained some numerical solutions to (5), a detailed comparison of perturbation solutions (like (7)) and computational solutions of (5) was not made. For example, one can verify the calculation of the second-order barotropic pressure correction (7b), or ask to what extent the simple interior form for V_c in (7a) holds. System (5a)–(5d) is solved as a two point boundary value problem using the Newton–Raphson–Kantorovich relaxation algorithm with eight homogeneous boundary conditions. The linear solution is used as an initial guess, along with an initial setting $P_b = 0$, which is appropriate for the antisymmetric linear solution since it has identically zero radial mass flux by itself. Once a nonlinear solution is found, it is used as a starting point for the next step in parameter space. In practice the method works well,

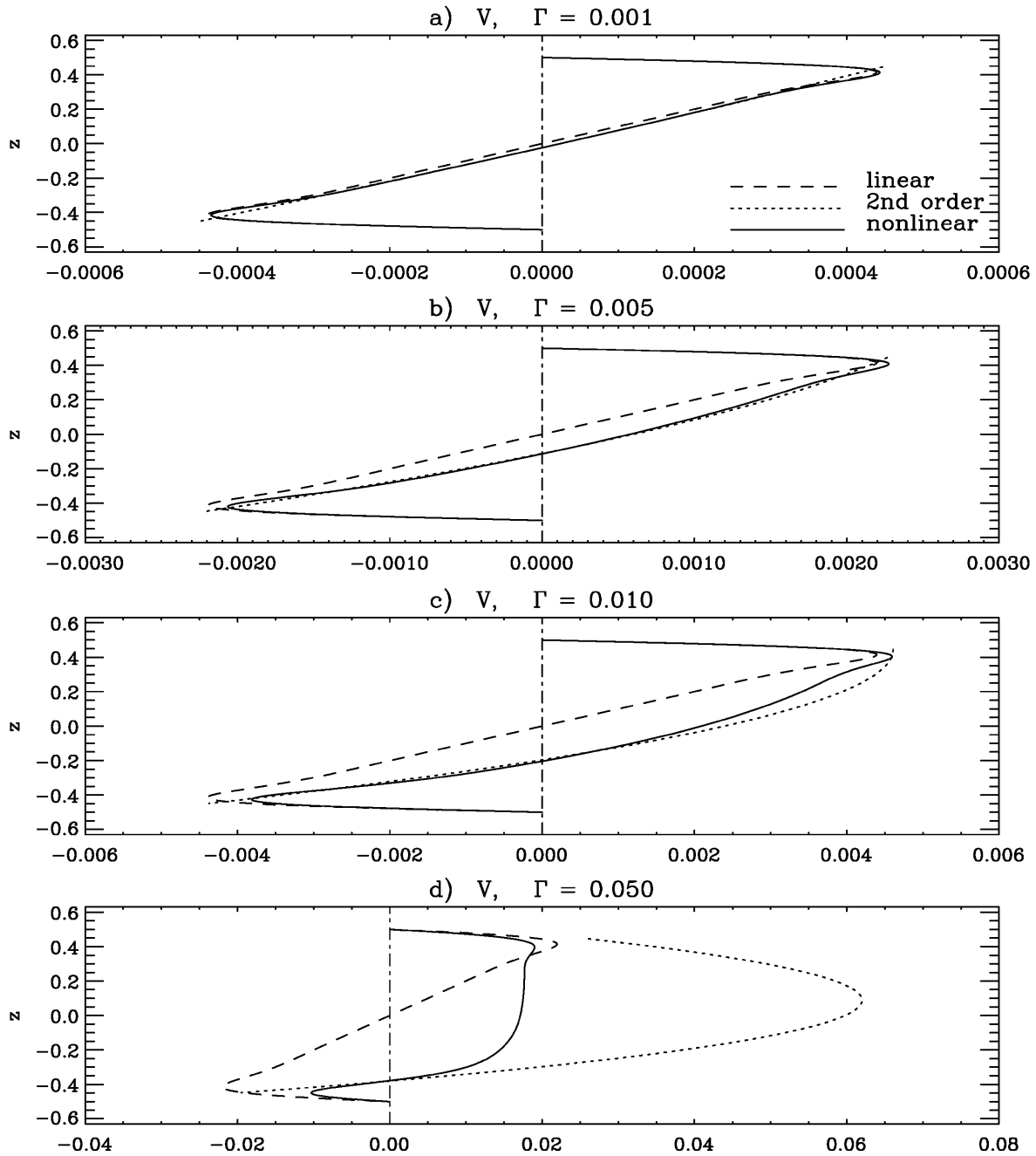


Figure 1. Azimuthal velocity from the self-similar model. The linear solution (valid at all Taylor numbers) and the second-order asymptotic theory (valid at large Ta) are included in the dashed and dotted lines, respectively. The solid line shows solutions of the nonlinear model equations (5). $Pr = 10$ and $Ta = 10^{10}$, $\Gamma = (0.001, 0.005, 0.01, 0.05)$ in (a)–(d), respectively.

converging in a few milliseconds when run on an SGI workstation. At the highest Taylor number studied (10^{12}) a nonuniform grid of 1601 spatial points, with concentration near the two boundaries, was employed.

Figure 1 compares the evolution of the weakly nonlinear theoretical and the computed azimuthal velocities ($V = V_C$) with at a modest value of $Ta = 10^6$. The linear solution (taking the lowest-order terms from (7) and appending the appropriate Ekman boundary layers) is satisfactory only for the case shown in Figure 1(a). The second-order asymptotic theory (displayed without its linear Ekman layers that are attached to the two plates) does much better. However, it too eventually fails as the core region away from the walls gives way to

a swirl velocity that becomes homogenized (i.e., vertically invariant) near the upper plate. When the Taylor number is raised to a substantially higher value, the sequence for increasing Γ is similar but the differences between theory and numerical solution of the ODEs occur at lower Γ . The plots in Figure 2 illustrate that both the swirl velocity and the total temperature become homogenized in the upper part of the cell, with strong thermal boundary layers appearing at the bottom. The weakly nonlinear theory works well in the $\Gamma = 0.001$ case, but in Figure 2(b), (c) both it and the linear model are so much in error that they are not plotted.

As Barcilon and Pedlosky (1967) and Homsy and Hudon (1969) illustrate, the transition between the linear (or weakly nonlinear) theory and the nonlinear states is governed by the composite parameter $\beta = \alpha\Delta T\text{Ta}^{1/4}\text{Pr}$, which represents the ratio of vertical thermal advection to thermal diffusion. For example, the midplane temperature starts to deviate significantly (at about the 10% level) from the linear solution when $\beta = \alpha\Delta T/Ta^{1/4}\text{Pr} \approx 4$. Figure 2(b), (c) illustrate the typical structure of the asymptotic nonlinear states at large values of β . The temperature is homogeneous in the interior with the value at the upper plate. A thermal boundary layer near the bottom plate reduces T to $-\frac{1}{2}$ at the bottom wall. This thermal boundary layer thins as the Prandtl number increases (hence higher β). We call these the thermocline modes of the nonlinear model. In these states the swirl is barotropic in the interior and the radial velocity effectively vanishes there. The shear in the swirl is concentrated in the thermal boundary layer at the bottom and in an Ekman layer at the top. The vertical velocity arises in the wall layers and is also invariant across the interior.

To review the basic physics of the thermocline modes and to isolate the Prandtl number dependence let V_i be the constant interior azimuthal velocity. This also serves as an azimuthal velocity scale for the boundary layers. The linear Ekman suction associated with the solid rotation accompanying V_i is just $W_i \approx 2V_i\lambda$. An estimate for the magnitude of the radial velocity in the boundary layers is, from (5d), $U_{bl} \approx V_i\lambda^2$. These scales show that the horizontal momentum equations are linear in the Ekman layers. The interior radial velocity $U_i < U_{bl}/\lambda$ to balance radial fluxes. Thus in the interior (5a) may be reduced because $\text{Ta}V \approx \lambda^4 V_i \gg U^2 \approx WU' \approx \lambda^2 V_i^2$. The strong inequality then results from the smallness of V_i (as indeed we shall see that $V_i \approx \Gamma \ll 1$), and the substantial size of λ for the rapidly rotating cases we are considering. Outside the Ekman layers the azimuthal equation (5b) balances vertical advection with vertical diffusion. Thus, the asymptotic dynamics are governed by

$$-U_c'' = V_c\text{Ta} - \Gamma\text{Ta}T_{\text{total}} - \text{Ta}P_b, \quad (8a)$$

$$-U_c - V_c'' = -W_c V_c' - 2U_c V_c, \quad (8b)$$

$$0 = T_{\text{total}}'' - \text{Pr}W_c T_{\text{total}}', \quad (8c)$$

$$W_c' + 2U_c = 0. \quad (8d)$$

In (8b) the right-hand side is negligible in the Ekman layer. Using the above ordering for W_i , (8c) shows that the total temperature (dynamic + conductive) will be constant in the interior when $\lambda\text{Pr}\Gamma$ is large (since then $T_{\text{total}}' \approx 0$). The sign of W_i determines the location of the thermal boundary layer, which has thickness $\delta_T \equiv 1/|\text{Pr}W_i|$. Since the upper plate is presumed hot, so $W_i < 0$, the thermal layer is attached to the lower plate and T_{total} elsewhere is just equal to the upper plate temperature $+\frac{1}{2}$, as seen in the numerical solutions of (5). Then (8a) and the linear Ekman suction at the bottom plate gives the interior solution:

$$T_{\text{total}} = \frac{1}{2}, \quad V_i = \Gamma/2 + P_b, \quad U_i = 0, \quad W_i = 2V_i\lambda = -\Gamma\lambda + 2\lambda P_b. \quad (9)$$

To complete the analysis we need to determine $P_b(\text{Pr}, \Gamma)$. This is done by matching the interior flow to the thermal and momentum boundary layers at the lower plate. If the thermal layer and the Ekman layer have similar thicknesses, then the solution structure near the lower plate appears analytically inaccessible because of the nonlinearity in the thermal equation. However, if $\text{Pr}\Gamma \gg 1$, then the thermal layer is embedded at the bottom side of the lower Ekman layer. Thus the interior solution extends through the bottom Ekman layer right to the outside of the thermal layer. The thermal layer is too thin to modify V substantially so the Ekman suction out of the bottom Ekman layer is unmodified. Its pumping is opposite to that coming down from the interior so that continuity of vertical velocity demands that $P_b \rightarrow \Gamma/2$ and $V_i \rightarrow 0$. The other limit, which has a nesting $1 \gg \delta_T \gg \delta_E \equiv 1/\lambda$, or $\text{Pr}\Gamma \ll 1$, has a thermal boundary layer that is outside the bottom Ekman layer. In the following paragraphs we derive some of the consequences of these two limits.

In the ‘‘small Prandtl number’’ ($\text{Pr}\Gamma \ll 1$) limit where the thermal layer is on the core (i.e., interior) side of the bottom Ekman layer, (8a) suggests we may approximate the solution *in the thermal layer* with

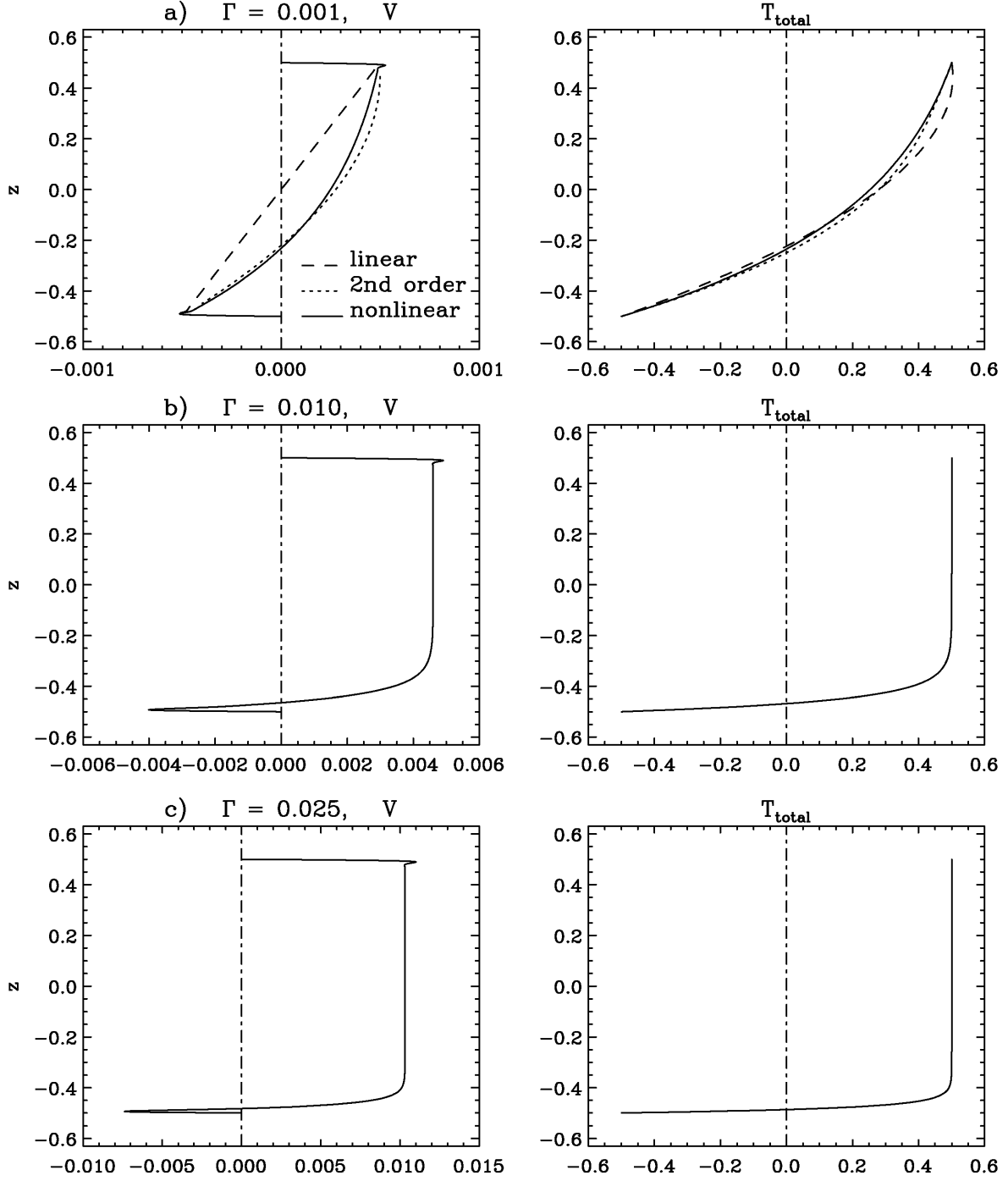


Figure 2. Azimuthal velocity and total nondimensional temperature T_{total} (including the conduction profile) for $\text{Pr} = 10$ and $\text{Ta} = 10^{10}$. $\Gamma = (0.001, 0.01, 0.025)$ in (a)–(c), respectively.

$$V_c = \Gamma T_{\text{total}} + P_b. \quad (10)$$

Then (8b) gives

$$U_c = \frac{V_c'' - W_c V_c'}{1 + 2V} = \frac{\Gamma [T_{\text{total}}'' - W_c T_{\text{total}}']}{1 + 2\Gamma T_{\text{total}} + 2P_b}. \quad (11)$$

Combining this with the thermal equation and using (8d) gives

$$U_c = \frac{\Gamma(\text{Pr} - 1)W_c T'_{\text{total}}}{1 + 2\Gamma T_{\text{total}} + 2P_b} = \frac{-W'_c}{2}.$$

This either can be integrated directly in order to obtain the functional relation $W_c(T_{\text{total}})$, or simply used to estimate the jump in W across the thermal layer. Assuming that $T_{\text{total}} \approx \frac{1}{2}$ and $P_b \approx O(\Gamma)$, the latter approach yields the fractional jump

$$\frac{\Delta W_c}{W_c} \approx 2\delta_T \Gamma(\text{Pr} - 1) \frac{1}{2\delta_T} \approx \Gamma(\text{Pr} - 1) \ll 1. \quad (12)$$

since Pr and Γ both are small. Thus W is effectively constant across the thermal layer so we can integrate (8c) to get

$$T_{\text{total}} = \frac{\coth(\text{Pr}W_i/2)}{2} - \frac{\exp(-\text{Pr}W_i z)}{2 \sinh(\text{Pr}W_i/2)}, \quad (13)$$

where the thermal field is assumed to asymptote to the core value above the bottom plate, and, because the thin Ekman layer cannot adjust the temperature field very much near $z = -\frac{1}{2}$, $T_{\text{total}} \rightarrow -\frac{1}{2}$ at $z = -\frac{1}{2}$. Thus (10) and (11) give a simple analytic formula for $V_c(z)$. Finally, evaluating \bar{V} at the bottom plate gives the Ekman suction at the bottom, $W_c(\frac{1}{2}) = -2\lambda(\Gamma/2 + P_b)$. This is matched to the interior vertical velocity, $2\lambda(\Gamma/2 + P_b)$, to get $P_b = 0$. This result is essentially the same as that derived by Hudson (1968).

The ‘‘large Prandtl number limit’’ ($\text{Pr} \gg 1$) has a different scaling, which is now outlined. The vertical velocity outside the Ekman layer at the bottom is still given by the last relation in (9). The boundary layer thickness for horizontal momentum is again just the Ekman layer thickness $\delta_E = \lambda^{-1}$. This is true no matter how motions in the Ekman layers are excited because rotation provides the only trapping mechanism for vorticity in this steady flow where the nonlinear terms (specifically the vertical advection) are small relative to the linear terms. Thus continuity provides an estimate for the size of the vertical velocity, $W \approx \bar{U}\delta_E = \bar{U}/\lambda$, where \bar{U} is the characteristic radial velocity across the Ekman layer that has thickness δ_E . We now estimate $\bar{U} \approx U'(z = -\frac{1}{2})\delta_E$. Integrating (8a) across the Ekman layer from the wall out to where the shear of the radial current vanishes gives

$$U'(z = -\frac{1}{2}) \approx \text{Ta} \int_{-1/2}^{-1/2+\delta_E} V_c dz + \text{Ta} \int_{-1/2}^{-1/2+\delta_E} [\Gamma T_{\text{total}} + P_b] dz.$$

The first term is small because $V_c \approx V_i \rightarrow 0$ (see below). The bracketed term is about $-\Gamma$ at the bottom plate and decreases to zero across the thermal layer, which, for $\text{Pr}\Gamma \gg 1$, has thickness $\delta_T \ll \delta_E$. Thus $\bar{U} \approx \text{Ta}\Gamma\delta_T\delta_E$ or $W \approx \Gamma\text{Ta}\delta_T\delta_E^2$. However, $\delta_T \approx 1/\text{Pr}W$ and $\text{Ta} \equiv 4\lambda^4$ so $W \approx \Gamma^{1/2}\lambda/\text{Pr}^{1/2}$. At large Prandtl number the vertical velocity into the bottom Ekman layer becomes small and can no longer balance that coming down from above unless V_i is much smaller than $\Gamma/2$. In fact, we see that $V_i \approx (\Gamma/\text{Pr})^{1/2}$ or $P_b = -\Gamma/2 + O(\Gamma^{1/2}\text{Pr}^{-1/2})$. The constant of proportionality in the latter expression is independent of λ .

Figure 3 shows numerical results illustrating the development of extremely thin thermal layers and a decrease of the interior swirl with Prandtl number in accord with the above scaling. Figure 4 suggests that, for $\Gamma = 0.05$, the large Pr limit for P_b , $P_b + \Gamma/2 \propto \text{Pr}^{-1/2}$, is approached as soon as $\text{Pr} > 10$. For small Pr , $P_b \rightarrow 0$, but because of the dual requirements $\text{Pr}\Gamma \ll 1$ and $\Gamma\text{Pr}\lambda \gg 1$ (to be in the thermocline regime), decreasing Pr to extremely small values at fixed Γ leads to some minor divergence from $P_b = 0$ in the small Prandtl number limit. In fact P_b goes slightly positive near the origin of Figure 4.

5. Computational Study of the Effects of a Sidewall

Although the similarity theory reviewed above is elegant and leads to relatively simple results, its applicability to flows in finite geometry has been questioned, particularly with respect to the potential for such motions to relax to the thermocline solutions (like (13)) in the interior when β is large. The thermocline mode has the peculiarity, noted by Barcilon and Pedlosky (1967), that the disk adjacent to the isothermal core region carries no heat flux, while that adjacent to the thermal boundary layer carries a substantial flux. With an insulating sidewall, this means that the corner region next to the former plate must have an even thinner

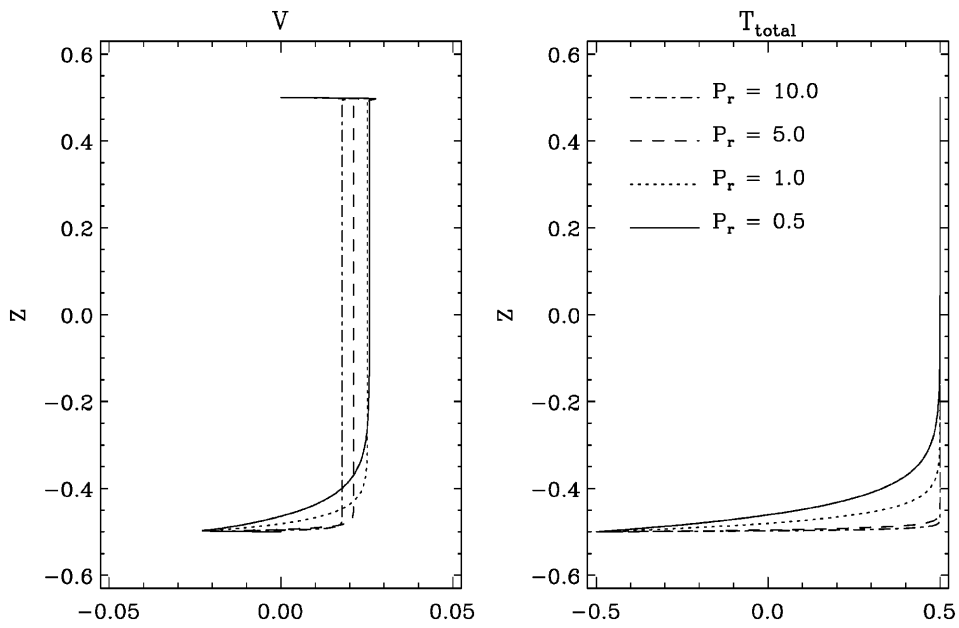


Figure 3. V and T for various Pr with $Ta = 10^8$ and $\Gamma = 0.01$.

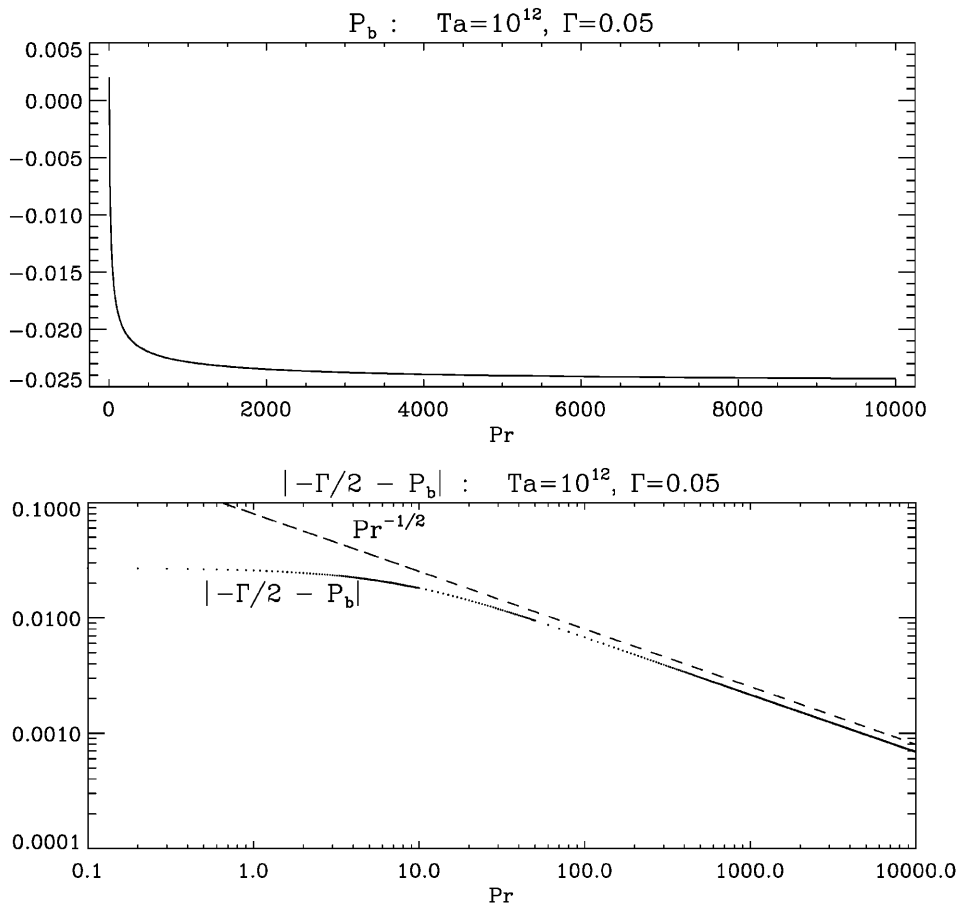


Figure 4. P_b versus Pr at $\Gamma = 0.05$ and $Ta = 10^{12}$. The lower plot shows the deviation of P_b from its asymptotic (large Prandtl number) limit $-\Gamma/2$.

thermal layer than that in the thermocline in order to balance the requirement that the total flux out of one plate equals the total flux into the other. It is not obvious that such a region confined only in the immediate vicinity of the sidewall exists.

Homsy and Hudson (1969, 1971) address this issue by finding analytic solutions to an approximate model, valid for large Froude number Fr (such as might be found in microgravity conditions), which is a generalization of (8c) to two dimensions. They consider a thermal balance between diffusion and *vertical* advection, namely,

$$\nabla^2 T = Prw \frac{\partial T}{\partial z}. \quad (14)$$

The basis for this model is that away from the immediate vicinity of the sidewall u is assumed to be small compared with w , so that horizontal thermal advection is neglected in (14). For axisymmetric motions, with small enough u , $dw/dz \approx 0$ so $w = w(r)$. The azimuthal velocity V is related to T by thermal wind balance, and w is related to T by applying the Ekman compatibility conditions $w \propto V_r$ just outside the two horizontal boundaries. Then one gets a nonlinear PDE for $T(r, z)$ alone. If $Fr \gg Pr\alpha\Delta T\lambda/8A$, which is of order ten for the parameters cited at the end of Section 3, this resulting PDE becomes linear. In this high Froude number limit Homsey and Hudson then obtain analytic solutions satisfying conducting or insulating boundary conditions at $r = R$, and show that these reduce to (13) as you leave the vertical wall region. Although suggestive of the utility of the similarity solution in physical systems with large rotational Froude number, this model does not address the situations typical of terrestrial laboratories where Fr is usually less than one.

Provided the inertial accelerations are small in the interior, and provided no sharp jets develop in V , then $w/u \sim \lambda \gg 1$, because while the vertical velocity is generated by Ekman pumping, the radial velocity is a result (in the linear situation) of a balance between Coriolis acceleration and diffusion. The dominance of vertical advection of temperature will fail if, for example, strong local azimuthal jets occur (leading to strong diffusion and large u). Alternatively, in the Ekman layers u is much larger than w , and thus if the outflow Ekman layer separates from the boundary the radial velocity in the interior will become large. Should this occur, one of the basic assumptions leading to (14) will again be violated. In either case, w must then be a function of r and z , u becomes significant, and horizontal advection of temperature cannot be neglected. Recall our focus on the gravitationally stably stratified case. If gravity is significant in the outer corners, then cold fluid being continuously centrifuged outward will pile up in a stable pool near the rim. The cold fluid can only move vertically and contact the upper hot wall if thermal diffusion is strong enough to allow a buoyancy layer of sufficient width to carry the appropriate flux. Otherwise the pool will spread laterally, and because most real situations will operate in a weakly diffusive regime, fluid motion will have to be along the isotherms. Thus the motion will parallel the edge of this cold pool, which is slanted, not vertical, and w will not dominate over u . If the cold pool is sufficiently dense, which can happen particularly if its formation is aided by having a cold outer rim, the outward Ekman layer motion at the bottom may actually separate near the edge of the cold pool and run upward at an angle toward the upper corner. In this instance the question of the validity of the self-similar thermocline solution then becomes related to the location, in r , at which the separation occurs.

We have looked at these issues by conducting computational simulations of the full axisymmetric equations:

$$\begin{aligned} \gamma_t + u\gamma_r + w\gamma_z &= \nabla_*^2 \gamma, \\ \eta_t + u\eta_r + w\eta_z + \eta\psi_z/r^2 - \text{Ta}\gamma_z^2/r^3 &= -\text{RaPr}^{-1}(T_r + \text{Fr}T_z A) + (\nabla^2 \eta - \eta/r^2), \\ T_t + uT_r + wT_z &= \text{Pr}^{-1}\nabla^2 T. \end{aligned} \quad (15)$$

In these equations ψ is the meridional streamfunction and $\eta = -\nabla_*^2 \psi/r$ is the azimuthal vorticity. γ is the absolute angular momentum per unit mass rV_{tot} , ∇^2 is the cylindrical Laplacian (for axisymmetric motion) and $\nabla_*^2 = \partial_r^2 + \partial_z^2 - (1/r)\partial_r$.

Equations (15) are solved on a uniform grid using second-order centered-differences in space and a second-order explicit predictor-corrector scheme for time. This code, and minor variations of it, has been extensively used for computations of isothermal rotating flows in cylinders (e.g., Lopez, 1996; Lopez and Weidman, 1996; Stevens *et al.* 1999). No slip boundary conditions are imposed on the top and bottom plates and at the sidewall (which all rotate at rate Ω). At $z = \pm\frac{1}{2}$, $T = \pm\frac{1}{2}$, while at $r = 1/A$ (the sidewall)

one of four possible conditions are imposed. The outer wall is: (a) insulating, (b) conducting with a linear temperature profile with temperatures matching those on the horizontal plates at the top and bottom, (c) hot with a temperature equal to that of the upper plate, or (d) cold with a temperature equal to that of the lower plate. That is,

$$T_r(r = A^{-1}, z) = 0, \quad T(r = A^{-1}, z) = z, \quad T(r = A^{-1}, z) = \frac{1}{2}, \quad \text{or} \quad T(r = A^{-1}, z) = -\frac{1}{2}, \quad \text{respectively.}$$

The typical resolution used for the results presented consists of 101 grid points in the vertical and $101/A$ grid points in radius, with a time step of 10^{-4} in units of the vertical diffusion time.

Results were obtained for a set of parameters typical of a terrestrial experiment. It is not practical to study motions over a wide region of the six-dimensional parameter space. We fix the Prandtl number at 7 (being typical of water or low viscosity silicone oil), and set the Taylor number to 1.56×10^6 so that the Ekman layers are thin and a relatively strong centrifugal buoyancy circulation can be generated (to put us in the thermocline regime). Two Rayleigh numbers were tried to get an indication of how the sidewall circulation varies as the buoyancy time scale is reduced relative to the dissipation time scales. Of most interest, however, is the question: How wide does the container have to be in order that a significant region of the cylinder have self-similar behavior? The aspect ratio is lowered from $\frac{1}{4}$ to $1/20$ while the depth H is held fixed. As the radius increases with H fixed, and all the other conditions are held constant, Ra and Ta are unchanged, but Fr increases.

Figure 5 illustrates the effect of varying the aspect ratio of the container at two different Rayleigh numbers. In this and all subsequent plots of this type, the axis is on the left and the sidewall is on the right. The figures show the meridional streamlines and the total temperature. In Figure 5 the sidewall boundary is an insulator. As expected, with higher Rayleigh number (which can be thought of as being obtained with a higher Γ , since Fr , Pr , and Ta are fixed) the thermal boundary layer near the axis collapses toward the bottom. As the cylinder is made wider, the region over which the isotherms are horizontal expands in radius, and in this region where $T = T(z)$ we anticipate that the similarity solution will be at least approximately valid. In all these solutions the isotherms slant upward into the upper right corner. There is little heat flux out of the top plate over most of its area where the adjacent fluid's temperature equals that of the lid (red). The flux into the bottom plate is balanced almost completely by conduction into the fluid in the upper right corner where the cold upwelled liquid comes into contact with the lid. Plots (not shown here) of $\partial T / \partial z|_{z=1/2}$ show that the vertical thermal gradient along the top plate peaks at the upper right corner for the insulating sidewall case, and near the corner for the other cases. $\partial T / \partial z|_{z=1/2}$ then falls smoothly to small values as the radius r approaches zero. The horizontal width of this upper thermal layer, as characterized by the width of the peak of $\partial T / \partial z|_{z=1/2}$ near $r = 1$, increases with Rayleigh number. In cases where the similarity solution does not apply, $\partial T / \partial z$ remains a function of r even at small radius. In the upper right corner region, the thermal boundary layer along the upper plate features a balance between vertical diffusion and advection (both horizontal and vertical).

In the wider container the cold pool at the bottom and near the rim reaches farther (in terms of height units) into the bulk. The cold pool also penetrates farther as the Rayleigh number is raised, reflecting the gravitational enhancement of relative stability associated with the strong stable stratification that develops near the rim. When the outer boundary is highly conducting, with a linear increase of temperature with height imposed, the circulation is similar in the bulk, but somewhat different near the rim (Figure 6). The cold pool in the lower right corner is not as strong because of the contribution of the wall to heating the pool. This means that the cold pool penetrates less far into the fluid, and the region of upward slanted flow is narrower. As in the insulated boundary case, the streamlines through the bulk are nearly vertical, indicating compliance with the $w(r)$ form postulated for interior motion in the self-similar rapidly rotating solutions. Ekman layers are present at each horizontal boundary.

Figures 7 and 8 contrast cases with a cold sidewall, with temperature equal to that of the bottom plate, with cases having a hot sidewall whose temperature is equal to that of the upper plate. In both these instances the sidewall has more influence on the global circulation than in the examples of Figures 5 and 6. In the coldwall case the direct gravitational circulation near the rim enhances the extent of the cold pool. In the aspect ratio $\frac{1}{4}$ case the centrifugal outflow Ekman layer separates (Figure 7(a), (b)). The separation point moves toward the axis at the higher Rayleigh number (7a) because the direct sidewall gravitationally driven component of the motion is stronger. When the outer rim is hot, the direct gravitational circulation assists

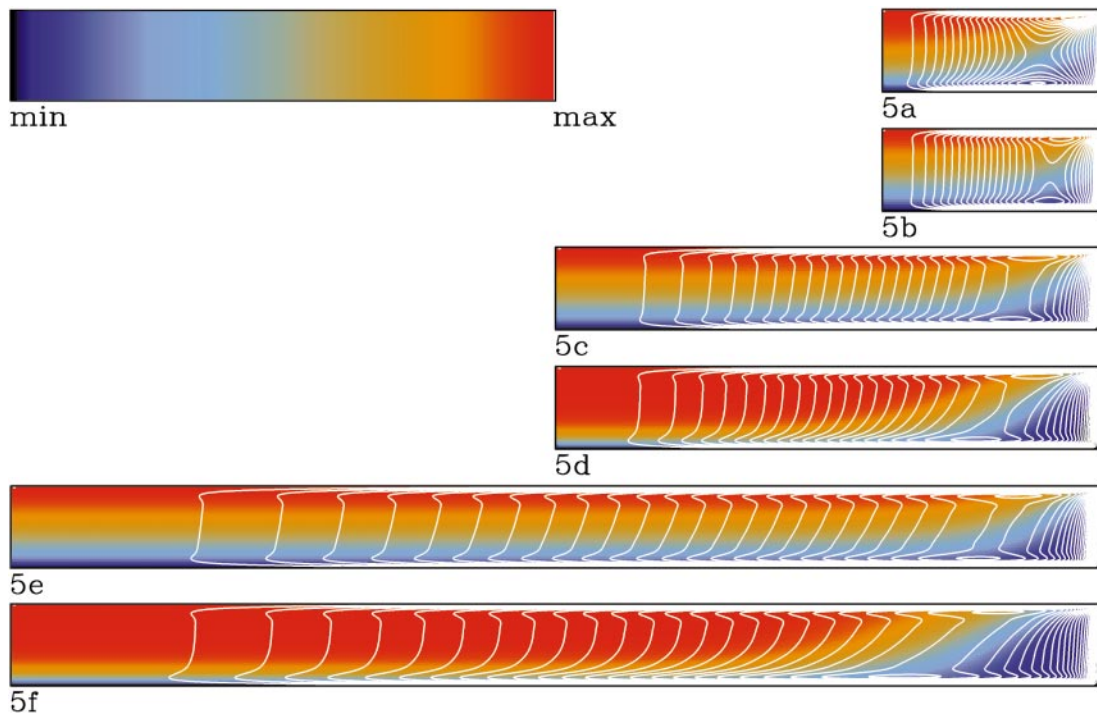


Figure 5. Streamlines for motion in the vertical plane, and temperature (color contours, blue = cold, red = hot), for an insulating sidewall boundary. In (a) $A = 1/4$, $Fr = 0.3$, $Ra = 7.5 \times 10^6$, $Ta = 1.56 \times 10^6$. (b) $A = 1/4$, $Fr = 0.3$, $Ra = 1.5 \times 10^6$, $Ta = 1.56 \times 10^6$. (c) $A = 1/10$, $Fr = 0.75$, $Ra = 1.5 \times 10^6$, $Ta = 1.56 \times 10^6$. (d) $A = 1/10$, $Fr = 0.75$, $Ra = 7.5 \times 10^6$, $Ta = 1.56 \times 10^6$. (e) $A = 1/20$, $Fr = 1.5$, $Ra = 1.5 \times 10^6$, $Ta = 1.56 \times 10^6$. (f) $A = 1/20$, $Fr = 1.5$, $Ra = 7.5 \times 10^6$, $Ta = 1.56 \times 10^6$.

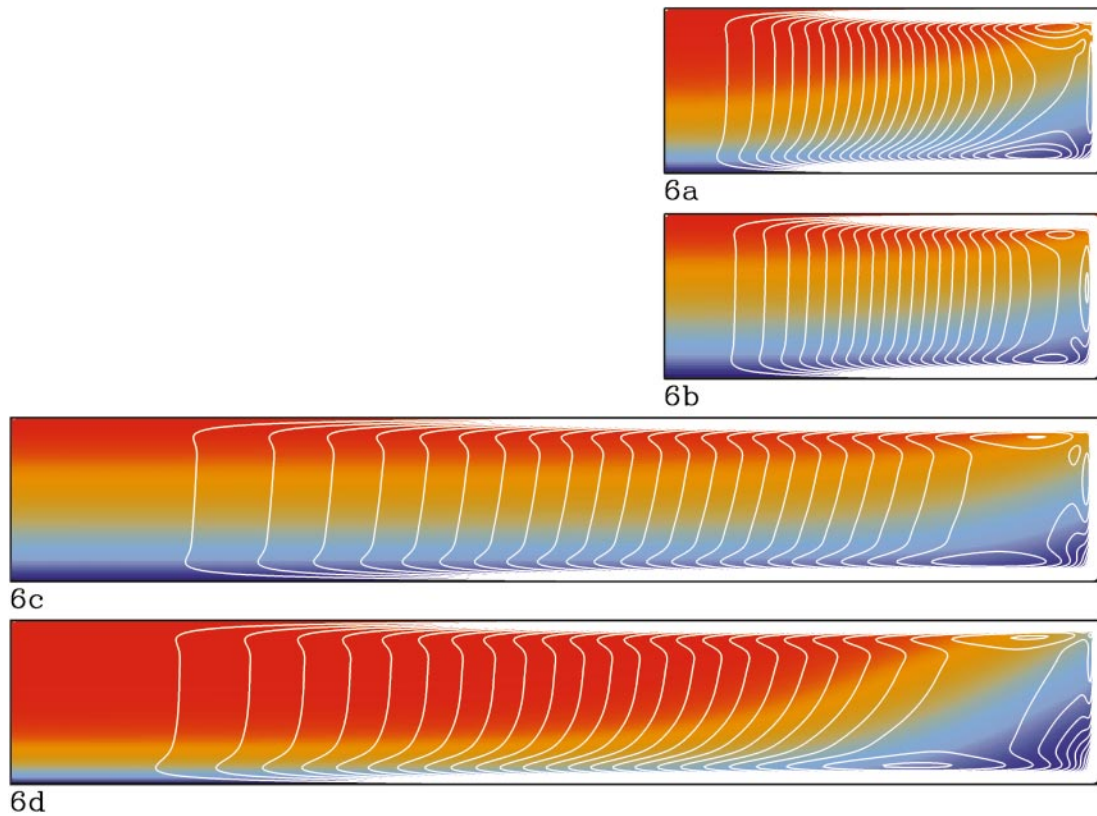


Figure 6. Same as Figure 5(a)–(d), except for a sidewall boundary with a linear temperature profile.

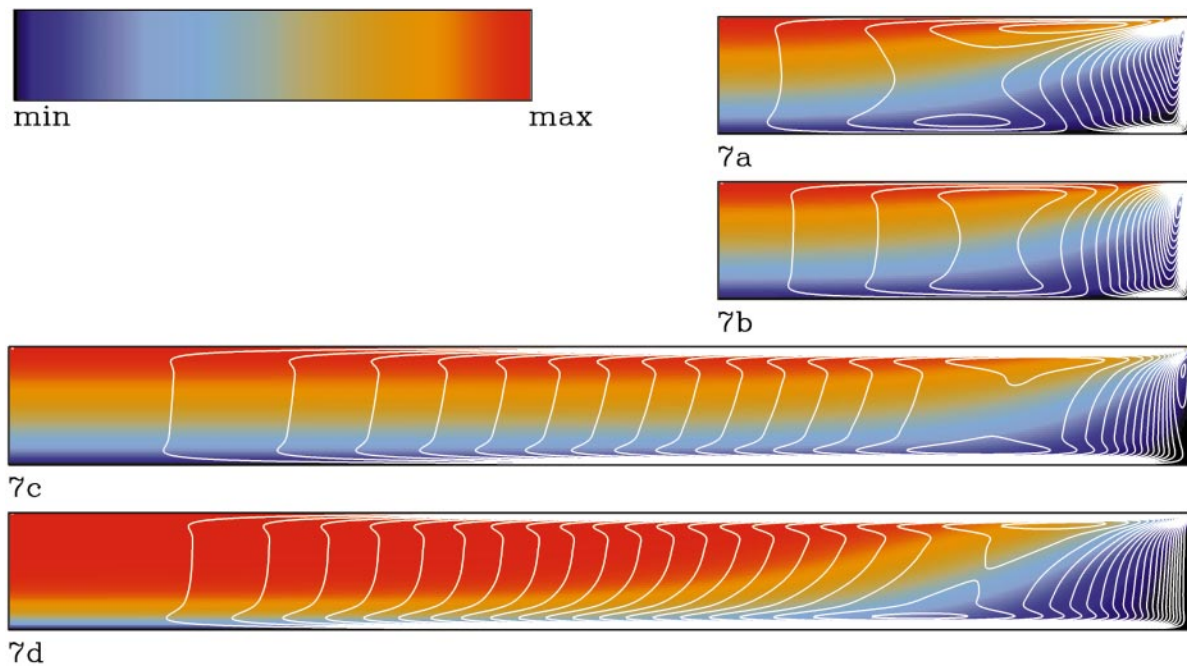


Figure 7. Same as Figure 5(a)–(d), except for a sidewall boundary that is cold.

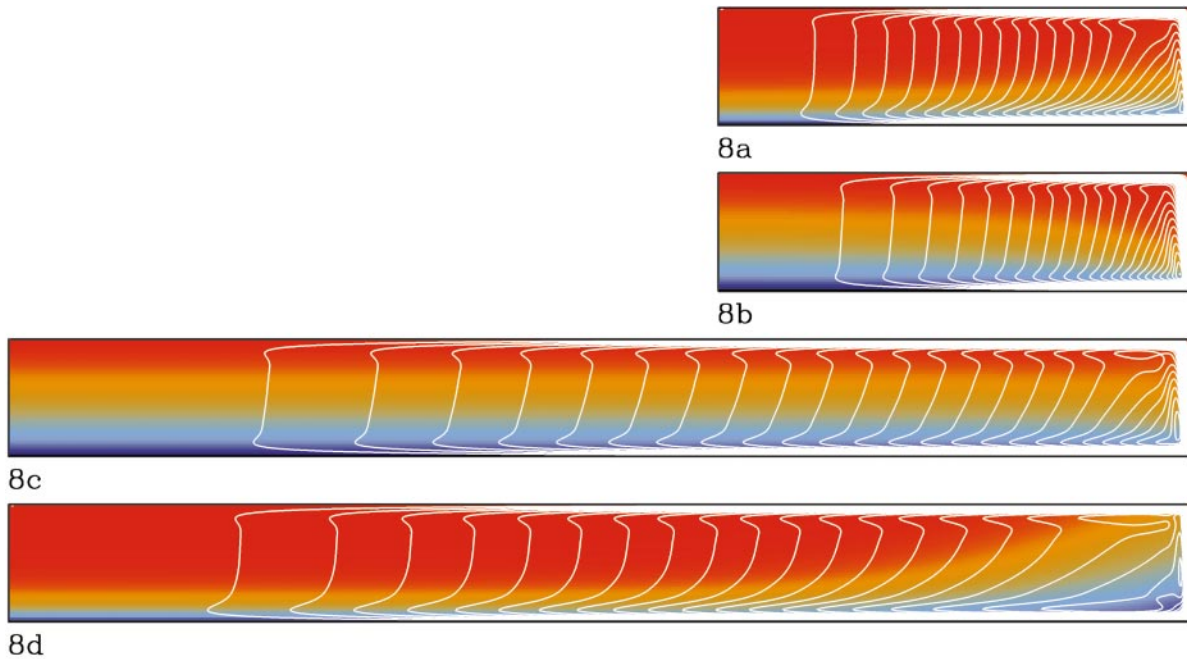


Figure 8. Same as Figure 5(a)–(d), except for a sidewall boundary that is hot.

the centrifugal cell. There are large differences in the near axis behavior (e.g., compare Figures 7(a) and 8(a)), especially when the aspect ratio is modest so the buoyancy driven part near the rim plays an effective role in setting the on-axis stratification.

The above plots show that for most of these computations the radial velocity is not everywhere negligible compared with the vertical velocity. In contrast to the model (14), radial heat advection is as important as vertical advection in these regions. For example, Figure 7(d) illustrates the tendency for the fluid sidewall

layer to move along the isotherms in regions about 80% out from the axis where the stratification (i.e., the thermal gradients) is strong. Where does the strong radial velocity in the interior (i.e., outside the Ekman layers) come from? The azimuthal equation of motion is

$$u(v_r + 2 + v/r) + wv_z = (\nabla^2 v - v/r^2).$$

This can be solved for u and then the terms that contribute to the radial velocity can be evaluated using the numerical results. Somewhat surprisingly the balance is primarily between Coriolis (the second term on the left) and frictional driving (the first term on the right). Advection becomes a source only in the upper right corner of the domain. The linear friction – Coriolis balance is the same as that used by Homsey and Hudson to argue that $u \ll w$. However, when the Froude number is order one, gravity is significant. Therefore in the regions of strong horizontal gradient (e.g., at $r \sim 0.8R$ in Figure 7(d)) there will be very large vertical shears of the azimuthal velocity v via thermal wind balance. Strong zonal jets develop out near the rim, and even weak diffusion of these leads to substantial radial velocities.

Figure 9 makes quantitative comparisons between the self-similar solutions and the steady-state integrations for the full axisymmetric motion including the sidewall. Because the Prandtl number is moderately large (7) the thermal field is most affected by advection and provides the most stringent test of the theory. In each plot the analytic curve is from (10), while the curve labeled ODE represents results from the numerical solution of the full nonlinear self-similar model (5). In all instances the asymptotic relation (14) overestimates the thermal gradients obtained from the ODE system. The results from the PDE solver are given at several radial positions located at the given fractional distance out from the axis to the wall (here at $r = 1$, independent of A). Figure 9(a) shows poor comparison in the 1/4 aspect ratio container. However, at aspect ratio 1/10, Figure 9(b) illustrates that over half the container is accurately self-similar. At an aspect ratio of 1/20, Figure 9(c) shows that the numerical solution of the nonlinear self-similar ODEs almost exactly describes the thermal field out to $r = 0.7R$ or so. Cases with linear and cold-wall and hot-wall boundary conditions have a qualitatively equivalent behavior. There are strong divergences from theory unless $A < 1/10$.

6. Conclusions

In flow between two infinite rotating parallel disks maintained at different temperatures centrifugal buoyancy expels fluid radially near the cold disk and moves it inward near the hot disk. The three parameters in the infinite disk problem are the Taylor number, the Prandtl number, and the density deficit parameter $\Gamma \equiv \alpha\Delta T/4$. A Boussinesq liquid is considered ($\alpha\Delta T \ll 1$). As noted by Hudson (1968), the infinite plate problem is amenable to a similarity transformation in which the variables are written as $T = T(z)$, $w = w(z)$, and $v = rV(z)$. When $\beta = \alpha\Delta T\text{Ta}^{1/4}\text{Pr} \lesssim 4$ the flow is reasonably well described by quasi-linear solutions of the governing ODEs. At larger values of β the vertical advection of heat becomes dominant over diffusion, and the vertical motion efficiently homogenizes the interior. The internal core thermal field becomes isothermal and equal to the hot plate temperature, while the core azimuthal velocity becomes barotropic (depth invariant). There is a strong thermal boundary layer, or thermocline, near the cold boundary. Because of the special symmetry imposed for the infinite radial geometry, gravity, however large, has no effect on these solutions.

In finite geometry, with a vertical sidewall at $r = R$, the thermal field must become dependent on radius, and gravitational buoyancy generation of azimuthal vorticity comes back into play. When the Froude number $\text{Fr} \approx \Omega^2 R/g \approx O(1)$ the important question is whether or not the gravitationally induced motion near the sidewall will invalidate the similarity solution over the bulk of the container. We investigated this by comparing numerical solutions of the full axisymmetric problem with analytically or numerically determined solutions to the simplified system obtained using the similarity reduction. For typical laboratory parameter values ($\text{Pr} = 7$, $\text{Ra} \sim 10^6$, $\text{Ta} \sim 10^6$, $\text{Fr} \sim 0.5$) these comparisons show that the similarity solutions do describe the motions over three-quarters, or so, of the inner part of the cylinder provided that the aspect ratio H/R is small (< 0.1 or so). The presence of a cold sidewall forces the lower boundary layer to separate, leading to a two cell circulation. The insulating and linear sidewall solutions feature a single vertical cell and strongly sloped streamlines near the rim, in which fluid angles up from the lower plate into the upper corner. Most of the heat flux through the upper plate occurs in the vicinity of the upper corner.

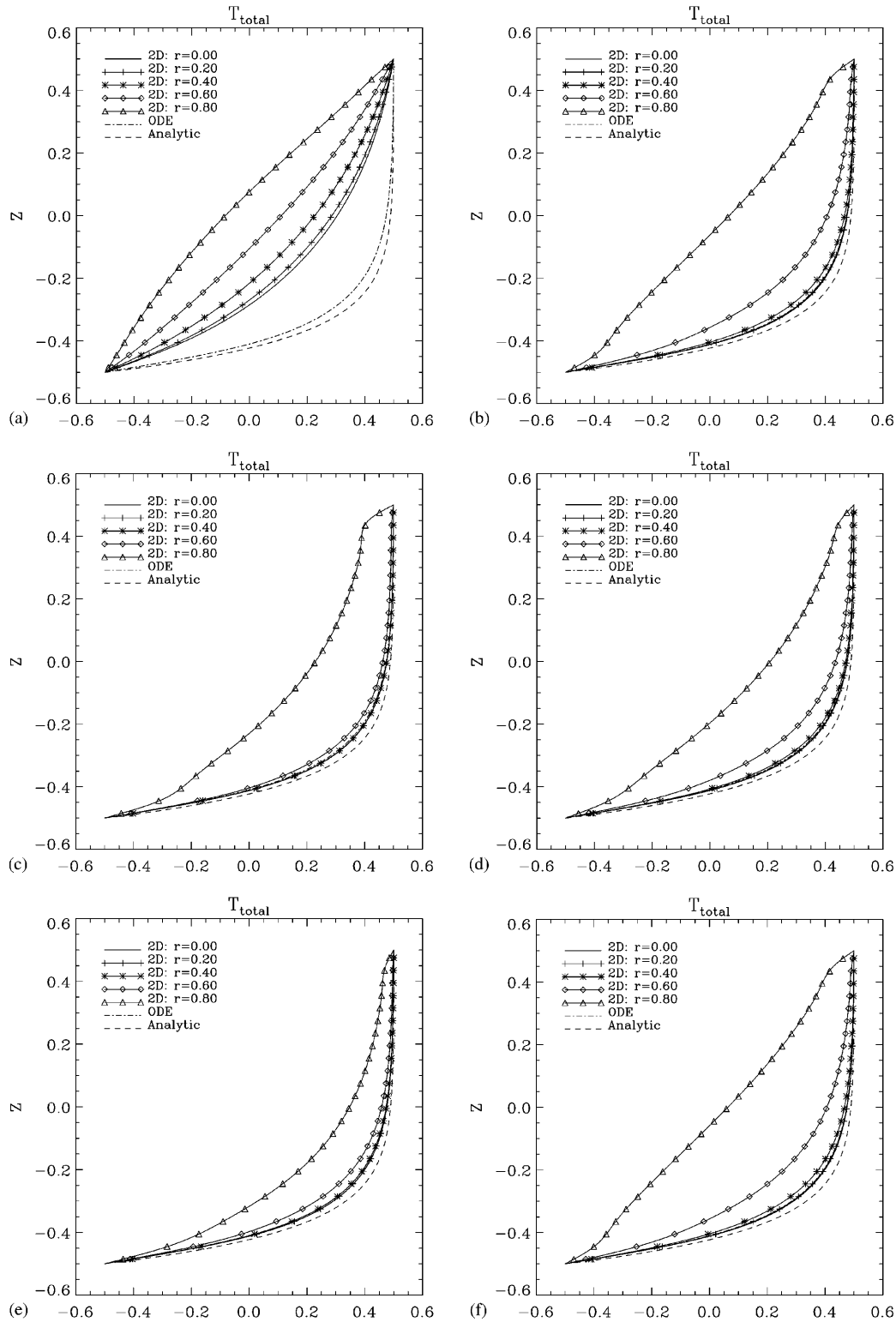


Figure 9. Comparison of similarity solution $T(z)$ obtained from asymptotic theory (10) and from numerical integration of (5) with results from axisymmetric simulations in a finite container. Soundings are compared at radial locations ranging from the axis ($r = 0$) to a location about 80% to the rim ($r = 0.8$). (a) As in Figure 5(a), insulating sidewall; (b) as in Figure 5(d), insulating sidewall; (c) as in Figure 5(f), insulating sidewall; (d) as in Figure 6(d), linear T on the sidewall; (e) as in Figure 7(d), cold sidewall; and (f) as in Figure 8(d), hot on the sidewall.

The gravitational circulation generated by a hot sidewall aids that induced by centrifugal buoyancy and produces a stronger than normal thermocline. Again sloping streamlines are the rule in the neighborhood of the rim. This situation is distinct from previous theories that neglect the radial velocity in favor of the vertical velocity induced by Ekman suction, and so have associated streamlines that are vertical all the way up to a very narrow sidewall boundary layer. While the radial velocity still reflects a balance of Coriolis acceleration and viscous diffusion, the thermal equation involves the full nonlinear advective–diffusive balance.

The simple thermocline solution should be observable in the terrestrial laboratory in a realistically wide (height/radius $\sim 1/10$, say) container. Of course, the present study assumes axisymmetry, and such experiments would be useful to elucidate the stability of such flows. Especially intriguing is the possibility of baroclinic instability near the rim. The present computational simulations predict that an azimuthal jet with strong vertical shear should arise in the sloping thermocline near the sidewall. Studies of this system, as well as the related one in which the top heated disk rotates differentially, are of interest because such flows serve as models for coastal currents in the oceans.

References

- Barcilon, V., and Pedlosky, J. (1967). On the steady motions produced by a stable stratification in a rapidly rotating fluid. *J. Fluid Mech.*, **29**, 673–690.
- Batchelor, G.K. (1951). A note on a class of solutions of the Navier–Stokes equations representing steady rotationally-symmetric flow. *Quart. J. Mech. Appl. Math.*, **4**, 29–41.
- Duncan, I.B. (1966). Axisymmetric convection between two rotating disks. *J. Fluid Mech.*, **24**, 417–449.
- Homsy, G.M., and Hudson, J.L. (1969). Centrifugally driven thermal convection in a rotating cylinder. *J. Fluid Mech.*, **35**, 33–52.
- Homsy, G.M., and Hudson, J.L. (1971). Centrifugal convection and its effect on the asymptotic stability of a bounded rotating fluid heated from below. *J. Fluid Mech.*, **48**, 605–624.
- Hudson, J.L. (1968). Non-isothermal flow between rotating disks. *Chem. Eng. Sci.*, **23**, 1007–1020.
- Lopez, J.M. (1996). Flow between a stationary and a rotating disk shrouded by a co-rotating cylinder. *Phys. Fluids*, **8**, 2605–2613.
- Lopez, J.M., and Weidman, P.D. (1996). Stability of stationary endwall boundary layers during spin-down. *J. Fluid Mech.*, **326**, 373–398.
- Rogers, M.H., and Lance, G.N. (1960). The rotationally symmetric flow of a viscous fluid in the presence of an infinite rotating disk. *J. Fluid Mech.*, **7**, 617–631.
- Stevens, J.L., Lopez, J.M., and Cantwell, B.J. (1999). Oscillatory flow states in an enclosed cylinder with a with a rotating endwall. *J. Fluid Mech.*, **389**, 101–188.